DNA adsorption by nanocrystalline allophane spherules and nanoaggregates, and implications for carbon sequestration in Andisols

Yu-Tuan Huang[a,1], David J. Lowe[a*], G. Jock Churchman[b], Louis A. Schipper[a], Ray Cursons[a], Heng Zhang[a], Tsan-Yao Chen[c], Alan Cooper[d]

[a] *School of Science, University of Waikato, Private Bag 3105, Hamilton 3240, New Zealand*

[b] *School of Agriculture, Food and Wine, University of Adelaide, Private Mail Bag No. 1, Glen Osmond, South Australia 5064*

[c] *Department of Engineering and System Science, National Tsing Hua University, Hsinchu, Taiwan 30013*

[d] *Australian Centre for Ancient DNA, School of Earth and Environmental Science, University of Adelaide, South Australia, Australia 5005*

Applied Clay Science

FINAL PRE-PUBLICATION VERSION 11 November 2015

Citation:
Huang, Y.-T., Lowe, D.J., Churchman, G.J., Schipper, L.A., Cursons, R., Zhang, H., Chen, T.-Y., Cooper, A. 2016. DNA adsorption by nanocrystalline allophane spherules and nanoaggregates, and implications for carbon sequestration in Andisols. *Applied Clay Science* 120, 40-50. (http://dx.doi.org/10.1016/j.clay.2015.11.009)

*Corresponding author. Tel.: +64 7 838 4438; fax: +64 7 856 0115
E-mail address: d.lowe@waikato.ac.nz (D.J. Lowe).

[1]Present address: *Department of Ecology and Environmental Science, Umeå University, SE-901 87 Umeå, Sweden*

Abstract

This study provides fundamental knowledge about the interaction of allophane, deoxyribonucleic acid (DNA), and organic matter in soils, and how allophane sequesters DNA. The adsorption capacities of salmon-sperm DNA on pure synthetic allophane (characterised morphologically and chemically) and on humic-acid-rich synthetic allophane were determined, and the resultant DNA-allophane complexes were characterised using synchrotron-radiation-derived P X-ray absorption near-edge fine structure (XANES) spectroscopy and infrared (IR) spectroscopy. The synthetic allophane adsorbed up to 34 μg mg^{-1} of salmon-sperm DNA. However, the presence of humic acid significantly lowered the DNA uptake on the synthetic allophane to 3.5 μg mg^{-1} by occupying the active sites on allophane so that DNA was repulsed. Both allophane and humic acid adsorbed DNA chemically through its phosphate groups. IR spectra for the allophane-DNA complex showed a chemical change of the Si−O−Al stretching of allophane after DNA adsorption, possibly because of the alteration of the steric distance of the allophane outer wall, or because of the precipitation of aluminium phosphate on allophane after DNA adsorption on it, or both. The aluminol groups of synthetic allophane almost completely reacted with additions of small amounts of DNA (~2−6 μg mg^{-1}), but the chemical adsorption of DNA on allophane simultaneously led to the formation of very porous allophane aggregates up to ~500 μm in diameter. The formation of the allophane nano- and microaggregates enabled up to 28 μg mg^{-1} of DNA to be adsorbed (~80% of total) within spaces (pores) between allophane spherules and allophane nanoaggregates (as "physical adsorption"), giving a total of 34 μg mg^{-1} of DNA adsorbed by the allophane. The stability of the allophane-DNA nano- and microaggregates likely prevents encapsulated DNA from exposure to oxidants, and DNA within small pores between allophane spherules and nanoaggregates may not be accessible to enzymes or microbes, hence enabling DNA protection and preservation in such materials. By implication, substantial organic carbon is therefore likely to be sequestered and protected in allophanic soils (Andisols) in the same way as demonstrated here for DNA, that is,

predominantly by encapsulation within a tortuous network of nanopores and submicropores amidst stable nanoaggregates and microaggregates, rather than by chemisorption alone.

Keywords:

Synthetic allophane, DNA adsorption capacity, Humic acids, Synchrotron radiation, Nanoaggregates, Carbon sequestration

Highlights:

- Synthetic allophane was able to adsorb up to 34 μg mg^{-1} of salmon-sperm DNA
- Adding humic acid to the synthetic allophane lowered its DNA uptake to 3.5 μg mg^{-1}
- The DNA-allophane complexes were characterised using P XANES and IR spectroscopy
- Stable microaggregates led to ~80% of DNA being occluded in tortuous nanopores
- Carbon in Andisols is protected in a network of nanopores thus its turnover is slow

1. Introduction

Andisols cover only approximately 0.8% of the ice-free surface in the world (Soil Survey Staff, 1999; McDaniel et al., 2012) but sequester upwards of ~1.8% of the total global soil carbon stocks (Matus et al., 2014; Takahashi and Dahlgren, 2016). Many Andisols are dominated by allophane and usually contain relatively large amounts of organic matter, up to ~ 8−12% organic carbon (McDaniel et al., 2012). Allophane is a nanocrystalline aluminosilicate with a formula $(1-2)SiO_2 \cdot Al_2O_3 \cdot (2-3)H_2O$ (Abidin et al., 2007; McDaniel et al., 2012) and it comprises hollow spherules ~3.5 to 5 nm in diameter with high specific surface areas (SSAs)[2] – from about 250 $m^2\ g^{-1}$ to as much as 1125 $m^2\ g^{-1}$ (e.g. Maeda et al., 1977; Parfitt et al., 1980; Wada, 1980; Allbrook, 1985; Parfitt, 1990; Ohashi et al., 2002; Iyoda et al., 2012). The high organic carbon content generally is significantly correlated with allophane content and SSA (Chevallier et al., 2010; Parfitt and Yuan, 2012), and carbon turnover in Andisols is slower than in other soils (Torn et al., 1997; Parfitt, 2009). Hence it is commonly acknowledged that Andisols can not only adsorb substantial organic carbon but also protect it from degradation (Dahlgren et al., 2004; Goh, 2004; Calabi-Floody et al., 2014). Allophane spherules are reportedly crucial in enabling Andisols firstly to store organic carbon and secondly to strongly adsorb phosphate (Parfitt, 1989, 2009; Calabi-Floody et al., 2011; Yuan and Wada, 2012).

[2]All abbreviations are defined together at the end of the text.

Adsorption of organic matter by these Al-rich nanocrystalline minerals governs the mobility of organic matter in the Andisols (Harsh, 2012), and the chemical bonding between the active aluminol groups on allophane spherules and organic matter is then considered to allow carbon to be adsorbed and stored (Yuan et al., 2000; Buurman et al., 2007; Parfitt, 2009; McDaniel et al., 2012; Takahashi and Dahlgren, 2016). Moreover, allophane spherules tend to form clusters of sub-rounded "nanoaggregates" about 100 nm in diameter (Calabi-Floody et al., 2011), which could also stabilize organic carbon within aggregates and allow long-term carbon sequestration in allophane-rich soils (Six et al., 2000a; Blanco-Canqui and Lal, 2004; Lehmann et al., 2007; Chevallier et al., 2010).

Nanocrystalline aluminosilicates show a phosphate adsorption capacity up to two orders of magnitude greater than that of long-range-order phyllosilicates and Fe- and Al-oxides/hydroxides (Hesterberg, 2010). Andisols thus have a high affinity for deoxyribonucleic acid (DNA) (Hashizume and Theng, 2007; Saeki et al., 2010a, 2010b) as well as phosphate (Allbrook, 1983, 1985; Parfitt, 1989). The adsorption of DNA on clay minerals is one of the most important mechanisms of DNA retention in soils (Ogram et al., 1988; Paget et al., 1992), and allophane, along with organic matter, presumably could facilitate the preservation of environmental DNA in soils hence could, if extractable, enable reconstruction of past environments via the DNA preserved (Huang et al., 2012; Rawlence et al., 2014). Furthermore, Matsuura et al. (2014) have hypothesised that allophane is able to protect DNA and ribonucleic acid (RNA) from ultraviolet light and, using computer modelling, simulated the interaction between DNA and allophane. Their simulations illustrated that the DNA strands underwent elongation and the phosphate backbone of DNA altered after bonding to allophane (Matsuura et al., 2013), possibly as a result of chemical adsorption of DNA through its phosphate groups to aluminol groups at the wall perforations of allophane (Huang et al., 2014). However, a more detailed understanding of the adsorption mechanism of DNA on

allophane has not been developed, and the driving factor allowing allophane to adsorb more DNA than other clay minerals has remained vague, thus providing impetus for the studies reported here.

In natural allophanic soil systems, the humic substances associated with allophane strongly bind to DNA and immobilize it (Saeki et al., 2011). However, some studies have contrarily shown that clay from which organic matter has been removed adsorbs more DNA than organic-matter-rich clay (Cai et al., 2006, 2007). Hence the level of influence of humic substances and organo-minerals on DNA adsorption in allophanic soils has been controversial and requires further examination.

1.1. Hypothesis

In this study it is therefore hypothesised that DNA is adsorbed by allophane both chemically and physically, and "physical adsorption" of DNA within pores amidst allophane spherules and nanoaggregates (defined here as aggregated clusters of allophane spherules up to ~100 nm in size) or microaggregates (defined here as aggregated clusters of allophane nanoaggregates up to several hundred micrometres in size, after Elliot, 1986) brings about the exceptionally high DNA adsorption capacity of allophane and enables DNA to be preserved. To test this hypothesis, the interactions between well-characterised synthetic allophane, salmon-sperm DNA, and humic acids are examined using P X-ray absorption near-edge structure (XANES) spectroscopy. XANES spectroscopy has been widely used in soil science to analyse the species of molecules, the oxidation state of a targeted atom, and the binding geometry of this atom with surrounding atoms in a molecule (e.g. Hesterberg, 2010; Lehmann and Solomon, 2010; Terzano et al., 2010). As well, the structural alterations of DNA and allophane spherules after they bind to each other are determined using infrared (IR) spectroscopy, which has been extremely useful to characterise chemicals and to describe structural or molecular alteration of chemicals adsorbed on clays (e.g. Farmer, 1968;

Parfitt, 1989; Shin et al., 2004; Tahoun, 2014). Finally, the degree of aggregation/complexation of DNA and allophane are examined using high-resolution laser sizing.

The findings with respect to DNA provide a detailed mechanism to help explain carbon sequestration and its unique longevity in Andisols.

2. Materials and methods

2.1. Synthetic allophane

2.1.1. Allophane synthesis

Pure allophane was synthesised according to Ohashi et al. (2002) with two minor modifications as follows. The Si source, Na_2SiO_4, for synthetic allophane was replaced with Na_2SiO_3, and the alkalinity of the Si solution was adjusted by adding NaOH, given that the alkalinity of Si solution should be triple the Al molarity. The allophane precursor was made with a mixture of Si and Al solutions (at the same concentration but with an atomic ratio of Si/Al of 0.75) together with the addition of NaOH, and the precursor was incubated for 48 h. In the current study, two synthetic allophane products with 50 mmol L^{-1} and 100 mmol L^{-1} of initial solutions were prepared, and the products were labelled as *50-allophane* and *100-allophane*, respectively. After hydrothermal incubation for 48 h, the synthetic products were washed with deionised (DI) water until the pH became neutral. For the DNA adsorption experiments, the dispersed allophane in DI water was adjusted accurately to pH 6.5 and stored without drying.

178 *2.1.2. Allophane analysis*

179 Transmission electron microscopy (TEM) was employed to observe the morphology of the
180 synthetic allophane. For TEM images of the synthetic allophane, 10 µL of diluted allophane
181 dispersion was spread on a lacey formvar/carbon copper grid (200 mesh) followed by drying at
182 40°C for moisture removal. Two TEM facilities were used, a Philips CM30 TEM and a JEOL
183 TEM-3010 scanning TEM for images with varied magnifications. The synthetic allophane was
184 damaged and melted in a fairly short time under the X-ray beam because allophane is heat-sensitive,
185 and so the synthetic allophane was photographed as quickly as possible to avoid over-exposure of
186 the samples to X-rays.

187 As well as TEM-based morphological observation, the allophane content of the synthesised
188 product was determined. To accurately estimate its Si/Al ratio, the synthetic allophane was frozen
189 rapidly with liquid nitrogen followed by freeze-drying. The allophane content was estimated by
190 oxalate extraction of Al and Si and pyrophosphate extraction of Al (following Parfitt and Wilson,
191 1985; Blakemore et al., 1987). The results showed that the Al/Si ratio was 1.2 and the allophane
192 yield was 95% of the total product. The SSA of the synthetic allophane was analysed via the
193 Brunauer-Emmett-Teller (BET) method with nitrogen gas adsorption at -195°C (Brunauer et al.,
194 1938), and pore volume and pore size were evaluated via the Barrett-Joyner-Halenda (BJH) method
195 (Barrett et al., 1951).

196

197 *2.1.3. Preparation of humic-acid-laden synthetic allophane*

198 To understand the influence of humic substances on the adsorption of DNA on allophane,
199 the dispersed 50-allophane in DI water was incubated overnight with humic acid (Pahokee peat
200 humic acid standard, which was obtained from the International Humic Substances Society) to

allow humic acid (HA) adsorption on synthetic allophane. Prior to incubation, the dried HA powder was dissolved in diluted NaOH and then adjusted to pH 6.5 using 0.1M HCl, and the resulting solution was then centrifuged at 8000 rpm (11,325 g) to remove insoluble HA. After incubation, the allophane-HA complex was repeatedly washed with DI water three to five times to remove unbound HA. The allophane-HA complex was re-suspended completely and adjusted to pH 6.5 for the DNA adsorption experimentation.

2.2. Adsorption isotherm of salmon-sperm DNA on synthetic allophane

The double-stranded salmon-sperm DNA (Sigma-Aldrich product number D1626) was dissolved in sterile DI water to provide a 2 mg mL^{-1} DNA solution, and the DNA additions for adsorption experimentation were in the range of 0 to 200 µL. The DNA solution was added to two sterile 1.5-mL tubes, one containing a given volume of dispersed allophane in DI water comprising 10 mg of synthetic allophane, and the other sterile DI water of the same volume as used to disperse the allophane. The two tubes were centrifuged at 13,000 rpm (10,000 g) after shaking 3 h on a rotator at room temperature, and the supernatants were then collected and analysed spectrophotometrically at 260 nm for DNA concentration. The adsorbed DNA was calculated from the difference between the amounts of DNA with and without 10 mg of synthetic allophane. These experiments were conducted in triplicate.

The adsorptive affinity and maximum adsorption capacity of DNA on synthetic allophane were analysed using the Langmuir equation given below:

$$q = \frac{A_{max} \cdot k \cdot C}{1 + k \cdot C}$$

where q represents the adsorbed DNA, A_{max} is a constant representing the maximum adsorption capacity (monolayer coverage), k is an adsorptive constant which is often considered an affinity parameter or binding strength, and C is the equilibrium-dissolved concentration of DNA.

After removal of supernatant, the tubes with remaining allophane and salmon-sperm DNA complexes were placed in a vacuum desiccator for two days for drying, and the dried allophane-DNA complexes were stored at 4°C for further chemical analysis. DNA adsorption on HA-rich allophane was performed following the same procedure as above.

2.3. Phosphorus X-ray absorption near-edge structure (P XANES) spectroscopy

The salmon-sperm DNA-allophane complexes were examined and characterised via synchrotron radiation-based P XANES. To obtain optimum signal-to-noise ratios of spectra, the air-dried allophane-DNA complexes were ground finely for uniformity and they were then compressed into pellets to increase the intensity of X-ray absorbance. The pellets of dried salmon-sperm DNA and allophane-DNA complexes were mounted on stainless steel sample holders and held in place with Kapton tape which has no X-ray absorbance over the P X-ray absorption region. The P X-ray absorption spectra were collected at beamline 16A1 Tender X-ray Absorption Spectroscopy at the National Synchrotron Radiation Research Center (NSRRC), Hsinchu, Taiwan. The beam current under standard operating conditions is 300 mA, and a Si(III) double-crystal monochromator is used for incident X-ray energy selection at a resolution of $1.5-2.1\times10^{-4}$ $\Delta E/E$. For the samples used in the current study, the P X-ray absorption was carried out under fluorescence mode, along with the employment of a Lytle detector purged with nitrogen gas. The beam was optimised and calibrated in advance against the adsorption edge of metallic Zr at 2223 eV.

P XANES spectra for samples were collected with photon energies in the range 2106−2230 eV, which are 40 eV forward and 84 eV behind the P *K*-edge of 2146 eV, and two to three scans were completed for each sample to obtain a representative spectrum. Over the scanning region of 2138−2180 eV, an energy step size of 0.2 eV was used along with a dwell time of 4 s per step for elaborate analysis, and a step size of 0.5 eV and dwell times of 2 s were used for the remaining energy region. The spectra obtained were normalized and merged through the Athena program, an interface to IFEFFIT (version 1.2.11) (Ravel and Newville, 2005), and then plotted.

2.4. Infrared (IR) spectroscopy

IR spectra for samples were obtained using Fourier transform infrared (FTIR) microspectroscopy at beamline BL14A1 at the NSRRC. This beamline employs a Nicolet Magna 860 FTIR spectrometer equipped with a Continuum IR microscope (Spectra Tech), and the FTIR facility is configured with synchrotron light as an external light source for the spectrometer.

Pure salmon-sperm DNA, pure synthetic allophane, and aggregates of synthetic allophane with differing concentrations of salmon-sperm DNA spikes (see section 2.2) were placed on a holder for analysis. Experiments were performed under the ring operation of top-up mode. Samples were analysed by IR in a range of 4000−600 cm^{-1}, with the co-addition of 128 scans. A spectrum of background signal (e.g. gases and moisture in atmosphere) without samples was collected for background removal. Data collection and background removal were completed via the program OMNIC™, and spectra were then processed using OMNIC™ and OriginPro 8.

2.5. Size distribution of DNA-allophane complexes

To examine the aggregation of synthetic allophane after adsorbing DNA, salmon-sperm DNA of varied concentrations were added into 30 mL of dispersed synthetic allophane in DI water for DNA adsorption. After allowing 3 h for complexation, allophane-DNA complexes with various DNA additions were collected without precipitation or centrifugation. The size distributions of allophane-DNA aggregates were determined by a Malvern Mastersizer 2000 laser diffractometer. Samples were injected into a vigorous stirring unit to homogenize them before throughput into the main measurement system (Sochan et al., 2012). DI water was used as the dispersant, where the dispersant refractive index was 1.33. Particle refractive index was set consistently at 1.5 for all samples.

3. Results and discussion

3.1. Physical properties of synthetic allophane spherules

The electron micrographs showed the spherical morphology of the synthetic allophane (Fig. 1) and indicated that the spherules had an external diameter about 10−15 nm (no significant size differences between the 50- and 100-allophanes were observed) and a wall thickness of ~1 nm (Fig. 1c). The particle size of the synthetic allophane was somewhat larger (by about three times) than the reported size of ~3.5−5 nm for natural allophane spherules (Creton et al., 2008; Parfitt, 2009), probably attributable to the unconstrained growth of synthetic allophane in the laboratory setting (Churchman and Lowe, 2012). It was also observed under TEM that allophane spherules coalesced naturally to form allophane nanoaggregates ~50−100 nm in diameter, and the aggregates then formed networks of large porous allophane aggregates in the size range of hundreds of nanometres (Fig. 1d).

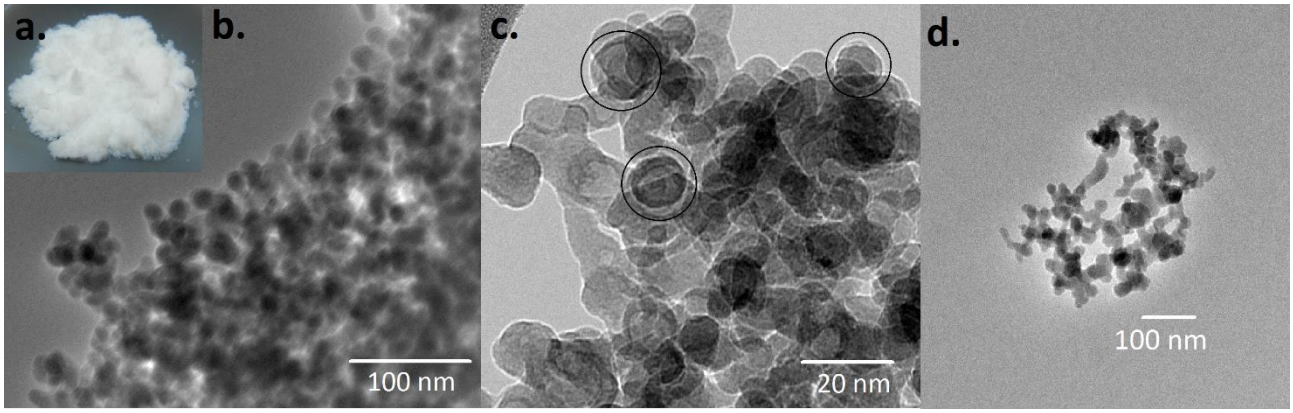

Fig. 1. Freeze-dried synthetic allophane (**a**) and the TEM images of the synthetic allophane showing the spherical and hollow morphology of allophane (**b** and **c**) as well as allophane nanoaggregates (**d**). The heat-sensitive allophane was damaged under the electron beam at high magnification, but the consistent spherical shape of allophane and the thickness of the allophane wall (in circles) are evident in photos b and c, respectively.

The discrete synthetic allophane spherules (equivalent to "particles" in the terminology of Bergaya and Lagaly, 2013, p.13) and their networks are in accordance with properties of natural allophanes observed in soils from New Zealand and Japan (Fig. 2) and elsewhere (Henmi and Wada, 1976; Maeda et al., 1977; Wells and Northey, 1984; Parfitt, 1990; Karube et al., 1996; Kaufhold et al., 2010; Delmelle et al., 2015). Karube et al. (1996) showed that unit particles of allophane formed domains ("primary floccules", which are referred to as nanoaggregates in the current paper) about 100 nm in diameter "like strings of beads" (Fig. 2c); and micrometre-sized clusters of allophane nanoaggregates (which are referred to here as microaggregates) in a dilute "suspension", analogous to the characteristics of synthetic allophane shown in Fig. 1d. Earlier, Allbrook (1985) suggested that surficial moisture films allow allophane spherules to remain discrete (even when aggregated) rather than conjoining into large micelles that characterise crystalline (platy) clays, thereby explaining the high porosity (and low bulk density) of allophanic soils.

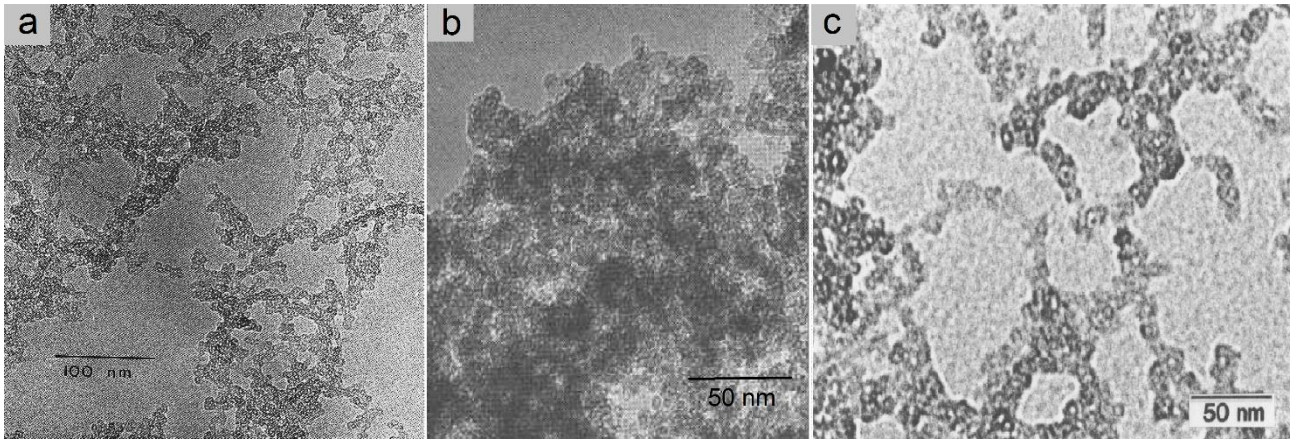

Fig. 2. Micrographs of natural allophane spherules occurring in **(a)** New Zealand, reproduced from Parfitt (1990), p. 345, with kind permission of CSIRO Publishing, Melbourne, Victoria, Australia, http://www.publish.csiro.au/nid/84/paper/SR9900343.htm (© CSIRO 1990); **(b)** Japan, reproduced from Henmi and Wada (1976), p.382, with kind permission of the Mineralogical Society of America; and **(c)** Japan, reproduced from Karube et al. (1996), p. 486, with kind permission of The Clay Minerals Society, publisher of *Clays and Clay Minerals*.

The spaces within the allophane nanoaggregates (inter-spherule spaces) were typically ≤ ~2 nm (according to measurements of the distances between spherules in TEM micrographs), whereas the spaces between the nanoaggregates (inter-nanoaggregate spaces) within microaggregates were of various sizes up to ~500 nm (see also Fig. 10C, below). The spaces (pores) could be further distributed into nanopores, which are defined here as < 100 nm in diameter, and submicropores which are ~100 to 500 nm in diameter. The high volume of nanopores and submicropores potentially allow the allophane aggregates to be highly porous and adsorptive (see section 3.5 below). Such numerous nanopores in Andisols were described by Chevallier et al. (2010) as having a fractal pore structure and therefore a pore network characterised by a high degree of tortuosity aptly called a "nanolabyrinth".

The estimated unit particle size of the synthetic allophane via BET was 16−23 nm (Table 1), slightly larger than the more accurate sizes estimated using TEM. The high pore volume of the two

synthetic allophane samples corresponded with the observations made using TEM, but the measured SSAs and pore volumes and pore sizes of 50-allophane and 100-allophane were somewhat different (Table 1). The SSAs for 50- and 100-allophane were 257 and 374 $m^2 g^{-1}$, and estimations of pore volume were 0.59 and 0.73 $cm^3 g^{-1}$, and of pore size were ~10 and ~8 nm, respectively. Allophane synthesised by Ohashi et al. (2002) using the same method and similar concentrations of Si and Al solutions as employed in the current study, possessed similar pore volumes, up to 0.78 $cm^3 g^{-1}$, but somewhat higher SSAs up to 550 $m^2 g^{-1}$. However, Kaufhold et al. (2010) reported a SSA of 348 $m^2 g^{-1}$ for synthetic allophane (made using the method of Ohashi et al., 2002) that closely matches that of the 100-allophane. The SSAs of some natural allophanes in New Zealand range from ~580 to 1125 $m^2 g^{-1}$ (Parfitt and Henmi, 1980; Allbrook, 1983; Parfitt, 1990). The differences in the SSAs of natural versus synthetic allophane are likely to have resulted from other colloids (e.g. organic matter, ferrihydrite, and halloysite) contributing a range of SSAs in the natural samples, and the SSAs for synthetic allophane are mainly influenced by the sizes of spherules (assumptions regarding monolayer coverage are also possible factors) (Allbrook, 1983; Parfitt, 1990). The higher adsorptivity of the 100-allophane than that of the 50-allophane presumably resulted from the higher concentrations of initial Si and Al solutions in making the 100-allophane, which led to relatively more numerous active aluminol groups on it. The nitrogen adsorption-desorption isotherms of two synthetic allophane products both showed hysteresis loops (Fig. 3), which are indicative of the presence of mesopores (2−50 nm in diameter) with capillary condensation within allophane samples (Neimark et al., 2000; Iyoda et al., 2012).

Table 1 Specific surface area and pore volume and pore size analyses of the two synthetic allophanes used in this study.

	50-allophane	100-allophane
Size of nanoparticles (nm)	23.31	16.02
BET surface area (m^2 g^{-1})	257	374
BJH pore volume (cm^3 g^{-1})	0.59	0.73
BJH pore size (nm)	9.92	7.67

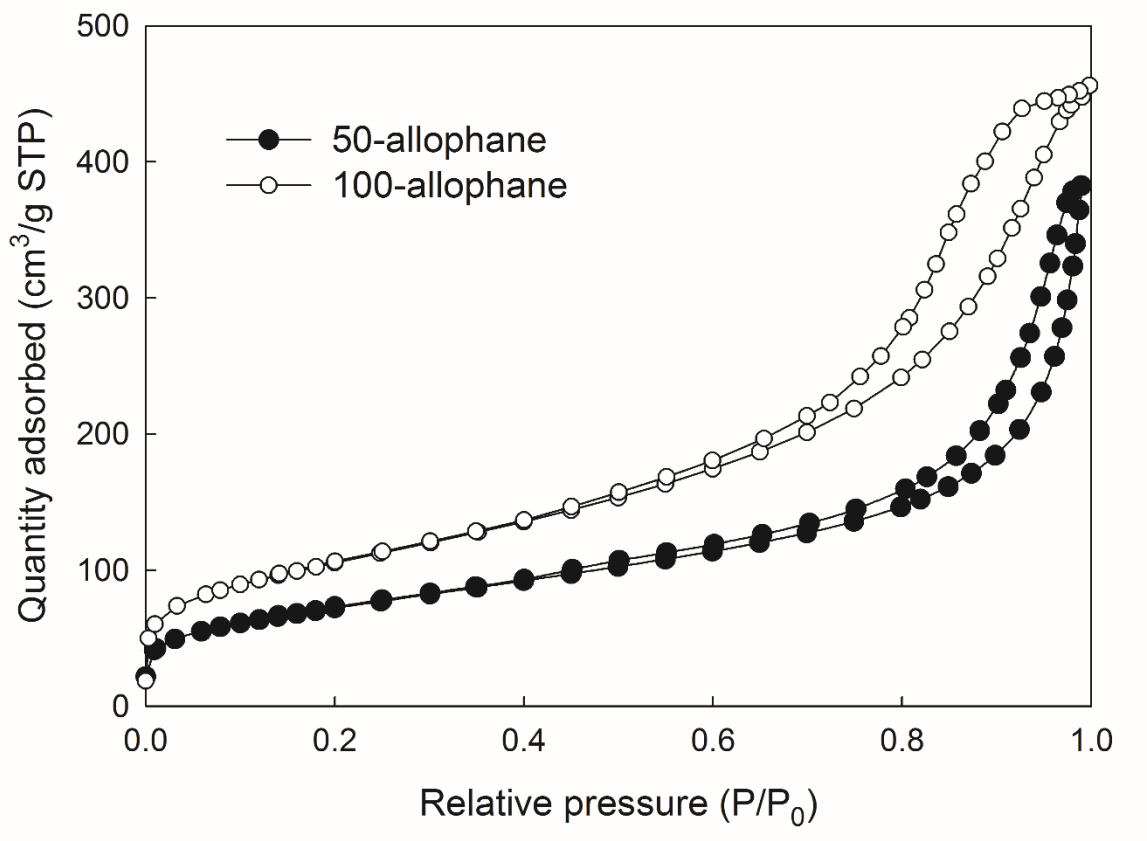

Fig. 3. N_2 gas adsorption-desorption isotherm on the two synthetic allophane products.

3.2. DNA adsorption capacity of synthetic allophane

The adsorption isotherms of salmon-sperm DNA on 50- and 100-allophane (Fig. 4) can be classified as *L*-shaped isotherms, which are characterised by a decreasing slope while concentration increases because the vacant adsorptive sites become covered and saturated (Sposito, 1989). The calculated adsorption maximum (A_{max}) of DNA by 100-allophane, with a comparatively high SSA

and pore volume, was 34 μg mg^{-1} allophane (adsorptive coefficient *k* was 0.0044), and A_{max} for DNA on 50-allophane was 26 μg mg^{-1} allophane (*k* was also 0.0044). That the 50- and 100-allophane both had the same adsorptive coefficients indicated that their surface adsorptive energies are similar. The adsorption isotherms both showed a rapid and strong adsorption of DNA on to allophane when DNA additions were low, followed by weakening adsorption whilst DNA additions increased. However, the different DNA adsorption capacities for 50- and 100-allophane (26 and 34 μg mg^{-1}, respectively) mainly resulted from the different numbers of active sites of the two materials.

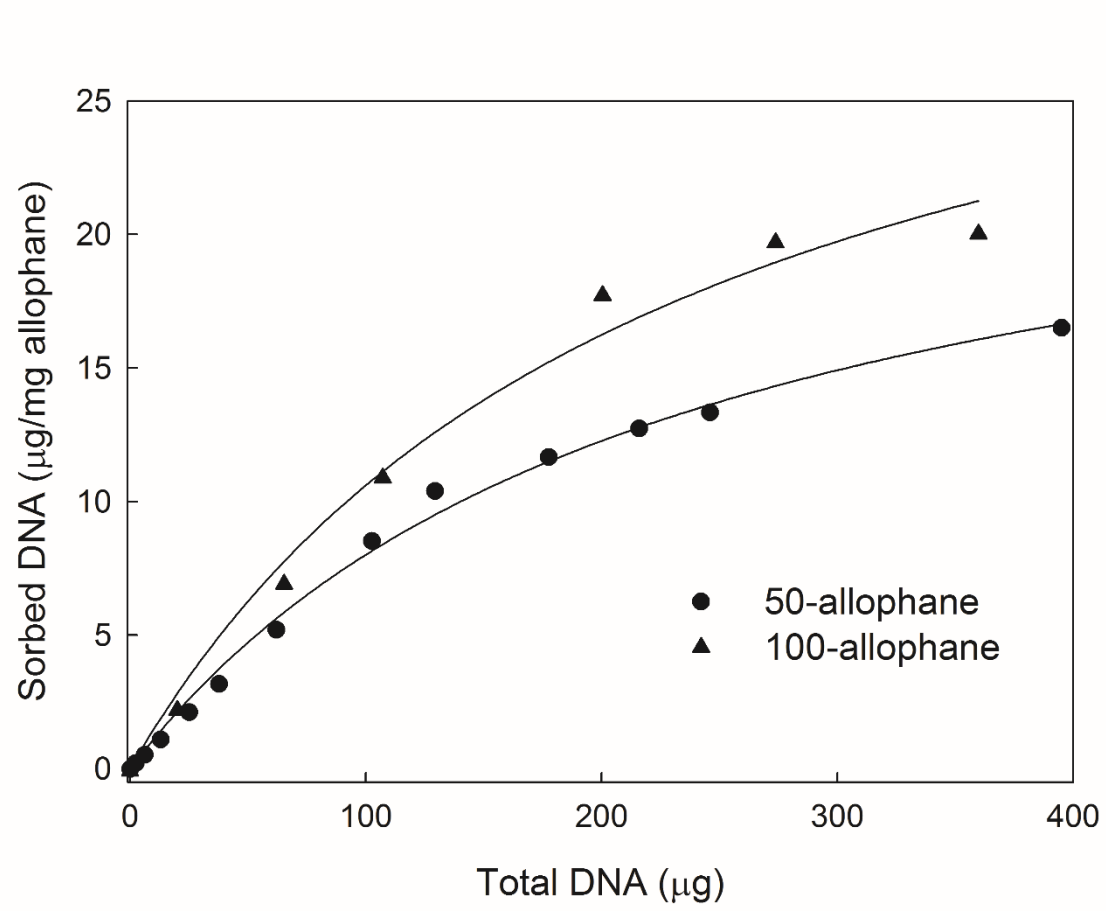

Fig. 4. Adsorption isotherms of salmon-sperm DNA on 10 mg of 50-allophane or 100-allophane. Reaction time was 3 h. The DNA adsorption isotherms were fitted to a Langmuir model, and the coefficients of determination (r^2) of Langmuir fitting for DNA adsorption on 50-allophane and 100-allophane were 0.987 and 0.995, respectively.

In contrast to the findings obtained here from DNA adsorption on moist synthetic allophane, Saeki et al. (2010a) reported the maximum DNA adsorption capacity for dried synthetic allophane at pH 6 to be only 5 μg mg^{-1}. Factors that influence the rate of DNA adsorption on allophane include acidity and ionic strength and also the moisture status of allophane. The drying process always generates non-reversible shrinkage of allophane aggregates and lowers the specific SSA (Rousseaux and Warkentin, 1976; Allbrook, 1992; Gray and Allbrook, 2002; Woignier et al., 2007; Kaufhold et al., 2010), potentially by ~40% according to Allbrook (1985). Consequently, it is concluded that drying would reduce DNA adsorption capacity of allophane and that it is ideal to keep synthetic allophane moist as a gel for subsequent applications.

3.2.1. Influence of humic acid on DNA adsorption capacity of 50-allophane

It was found that the presence of humic acid on the surface of synthetic 50-allophane significantly hampered the adsorption of DNA (Fig. 5), reducing the capacity from 26 to 3.5 μg DNA for 1 mg of synthetic allophane (note the 100-allophane had a maximum DNA uptake of 34 μg mg^{-1}). This result accords with those of Cai et al. (2006) and Saeki and Sakai (2009), who both showed that a decrease of organic matter raises DNA adsorption on clay minerals and colloid particles from soils. In the current study, the relatively low DNA adsorption on the humic acid-rich synthetic allophane indicated either that humic acid was competitive with DNA and/or that the humic acid had already occupied the active aluminol groups on surface of allophane and hence fewer adsorptive sites on allophane remained. This discovery – that humic acid effectively reduces the capacity of DNA adsorption by allophane – suggests that allophanic soils and paleosols, characterised typically by a high content of organic matter as noted earlier, may not be so favourable for DNA adsorption from a long-term perspective as previously considered.

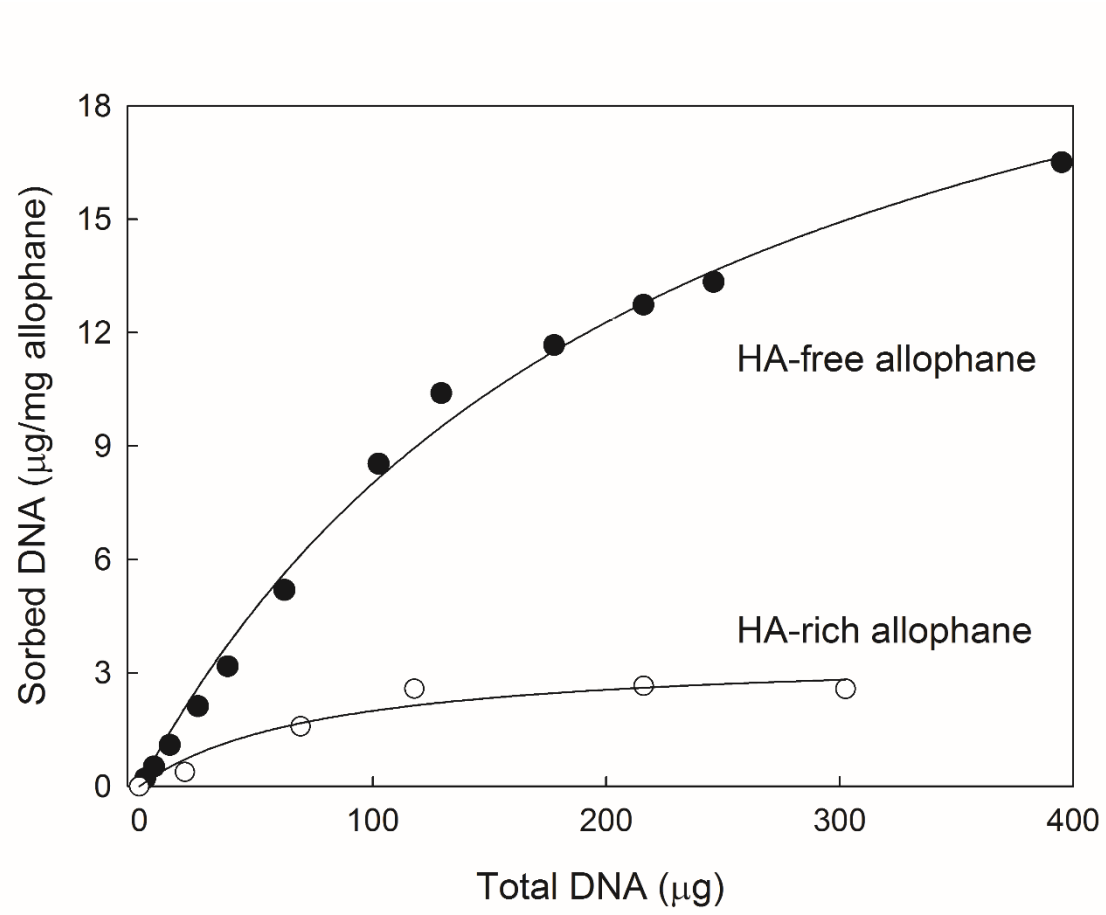

Fig. 5. The measured adsorption isotherms of salmon-sperm DNA on humic acid (HA)-free and HA-rich synthetic 50-allophane (both at pH 6.5) along with fitting to a Langmuir model (reprinted from Huang et al., 2014, p. 170, with kind permission of Springer). Each data point represents the average adsorption of samples in triplicate. The coefficients of determination (r^2) of Langmuir fitting for DNA adsorption on HA-free allophane and for HA-rich allophane were 0.995 and 0.946, respectively.

3.3. P XANES spectra for allophane- or humic-acid-associated DNA

The P XANES spectrum for pure salmon-sperm DNA (bold spectrum in Fig. 6) shows a sharp and strong white-line (WL) peak at 2153 eV, and a post-edge shoulder between 2160 and 2180 eV without showing pre-edge features. The P XANES spectrum for the allophane-associated DNA shows a pre-edge hump (2135–2141.1 eV) on the low-energy side of the absorption edge,

along with a slight shift of the WL peak from 2153.0 eV to 2153.3 eV (Fig. 6). The WL peak for the allophane-DNA complex could be attributed to the propagation of P 1s electrons into P(3p)−O(2p)−Al(3p) antibonding molecular orbitals (Khare et al., 2005) where the nuclei are repelled by positive charges of Al ions. In comparing the two XANES spectra, the positive shift of the WL peak for the allophane-associated DNA may be explained by the charge relocation from Al to P as a consequence of the strong electronegativity of DNA base pairs arising after the DNA was adsorbed chemically on to the allophane.

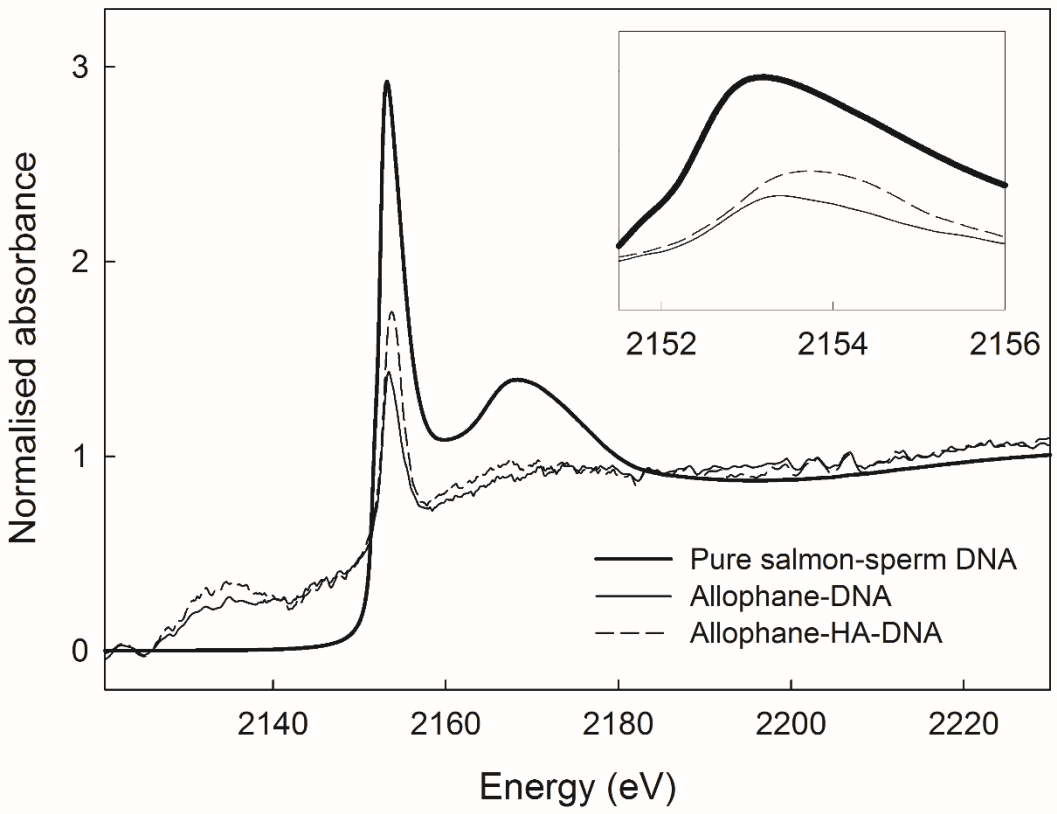

Fig. 6. Normalized P XANES spectra for pure salmon-sperm DNA, allophane-DNA complex, and allophane-HA-DNA complex. Two or three scans for one sample were obtained and then merged together for an average spectrum. The appended box shows detailed variations of spectra over the region of 2152−2156 eV.

426 The behaviour of salmon-sperm DNA adsorption on humic-acid-rich allophane was
427 illustrated by the P XANES spectrum as well (dashed spectrum in Fig. 6), whereby the WL peak for
428 humic acid-associated DNA was shifted forward to high energy relative to allophane-associated
429 DNA, along with amplified intensity of the WL peak and post-edge backscattering hump (see inset,
430 Fig. 6). The DNA bound to the humic acid covering the allophane characteristically showed not
431 only the chemical adsorption of DNA onto humic acid but also the oxidation of DNA molecules
432 because of the decoupling between phosphate ligands of DNA and the adsorptive sites of humic
433 acid, thereby confirming the high affinity of DNA and humic acid (Saeki et al., 2011). Accordingly,
434 it was expected that the adsorption of DNA on organo-allophane complexes would help to retain
435 environmental DNA in such soil materials. However, the negatively-charged humic acid (and its
436 ligands) atop allophane suppressed the charge relocation from phosphorus within the DNA
437 molecules to the adsorptive ligands of humic acid, a process illustrated by the higher WL intensity
438 for DNA bound to the humic-acid-rich allophane compared with the WL intensity for DNA on the
439 humic-acid-free allophane. Hence it is concluded that humic acid instead reduces DNA adsorption
440 in allophanic soils by not only attaching to active sites on the allophane spherules (thus precluding
441 DNA from binding) but also by repelling the negatively-charged phosphate groups in the DNA
442 molecules by electrostatic repulsion.

443 Even though humic acids inhibit the adsorption of DNA by allophane, the organo-allophane
444 complex in soils retains an ability to stabilize some environmental DNA by chemical adsorption and
445 possibly store the DNA indirectly. Using P XANES, Huang et al. (2014) analysed a natural
446 allophanic soil sample, to which salmon-sperm DNA had been added, in order to ascertain
447 specifically how DNA was adsorbed on allophane. However, the result was not conclusive because
448 it was unclear whether the added DNA was chemically bound to the allophane or to organics, or
449 both. In the present study, however, the spectrum from humic acid-associated DNA can be
450 distinguished from that for allophane-associated DNA. Accordingly, the distinct WL peak at 2153.8

451 eV for DNA associated with humic acid indicates that the salmon-sperm DNA added into the
452 natural allophanic soil (as reported by Huang et al., 2014) was in fact chemically bound to humic
453 acid or organics in soils rather than to the allophane spherules directly because the active sites on
454 allophane had been naturally occupied by organics.

455

456 *3.4. Infrared spectra for pure DNA, allophane, and DNA-allophane complexes*

457 The identifiable infrared spectral features from low wavenumbers for pure salmon-sperm
458 DNA (Fig. 7) correspond to P=O stretching (at 1098 cm^{-1}), O−P−O bending (at 1240 cm^{-1}), CH_2
459 and CH_3 bending (at 1300−1500 cm^{-1}), C=C stretching within amine bases (at 1450−1600 cm^{-1}),
460 C=O stretching within amine bases (at approximately 1700 cm^{-1}), and finally OH and NH stretching
461 (at 3000−3400 cm^{-1}) (Brown and Poon, 2005). With the use of infrared spectroscopy, the DNA
462 molecule was characterised mainly by absorbance of amine bases and phosphate groups, whereas
463 the absorbances of methylene bending, methyl bending, and aliphatic stretching were not distinct.
464 Freeze-dried synthetic allophane was characterised by strong infrared absorption between 900 and
465 1000 cm^{-1}, ascribable to the predominance of Si−O−Al bonds of allophane spherules and by the
466 medium absorption around 3000 to 3700 cm^{-1} relating to the hydroxyl groups on the surface of
467 allophane, together with the contribution of organic impurities near 1600 cm^{-1} (Parfitt and Henmi,
468 1980, 1982). After DNA adsorption on synthetic allophane, the addition of 0.2% salmon-sperm
469 DNA induced a steric alteration in Si−O−Al stretching of allophane: the strong absorption band at
470 1200 cm^{-1} of allophane was split into two broad sub-bands at 990 and 1080 cm^{-1} (bold line in Fig.
471 7), and the PO_2^- signal of the DNA molecule at 1240 cm^{-1} was not observed. The disappearance of
472 P−O stretching within the DNA molecule after it is bound to allophane supports the conclusion that
473 allophane binds to DNA through its phosphate groups (especially through the deprotonated P−O
474 sites). On the other hand, the alteration of Si−O−Al stretching of allophane after DNA adsorption

confirmed that DNA was attached to the reactive aluminol (AlOH) defects on the surface of allophane (Nanzyo, 1984; Parfitt, 1989), and the signal of Si−O−Al stretching shifted or disappeared because of the spatial inflexion of the allophane wall or because of the precipitation of aluminium phosphates (Parfitt, 1989) (or both).

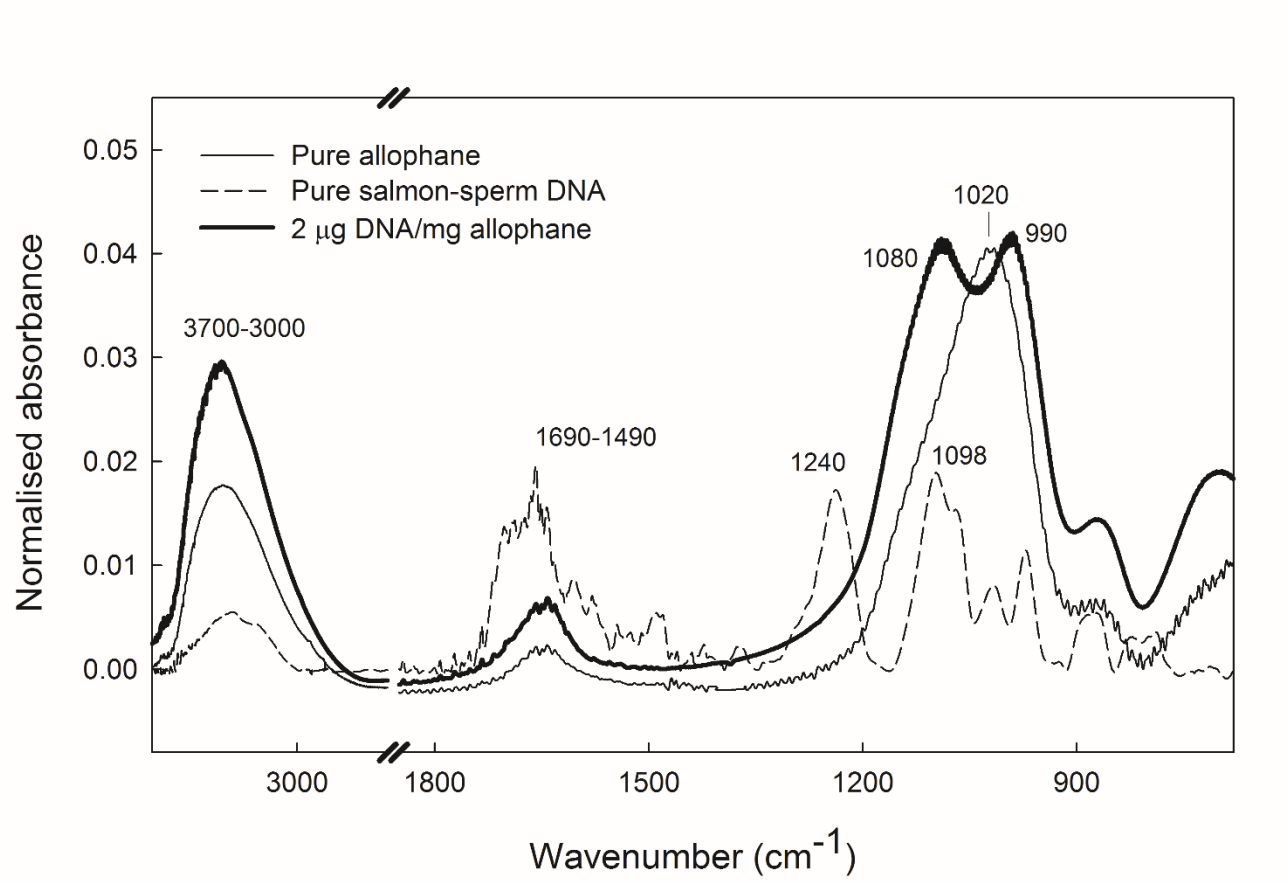

Fig. 7. Normalized infrared spectra for pure salmon-sperm DNA, synthetic allophane, and allophane-DNA complex. Identified spectral features at various wavenumbers correspond to OH group (3700−3000), C=C in the base planes of DNA (1690−1490), PO_2^- of DNA (1240), P=O (1098), and stretching Si−O−Al of allophane (1020).

With an increase in concentration of additional DNA (0.2, 0.7, and 1.1%) onto synthetic allophane, the intensity of the infrared absorption band at 1080 cm^{-1} increased and shifted gradually but the absorbance at 990 cm^{-1} remained the same (Fig. 8). Consequently, the absorbance at 990 cm^{-1} could be assigned to the chemical change of Si−O−Al bonding on the surface of allophane spherules after DNA adsorption because the peak at 990 cm^{-1} did not alter with the rising concentration of additional DNA. This result suggests that almost all the reactive defects of allophane spherules had reacted and altered chemically after the addition of only a small amount of DNA (e.g. 0.2% of DNA spike). More DNA, however, could still be taken up slowly even though the reactive sites had been saturated and would not change chemically further, and so other DNA adsorption mechanisms must have taken place to enable the uptake of more DNA by allophane.

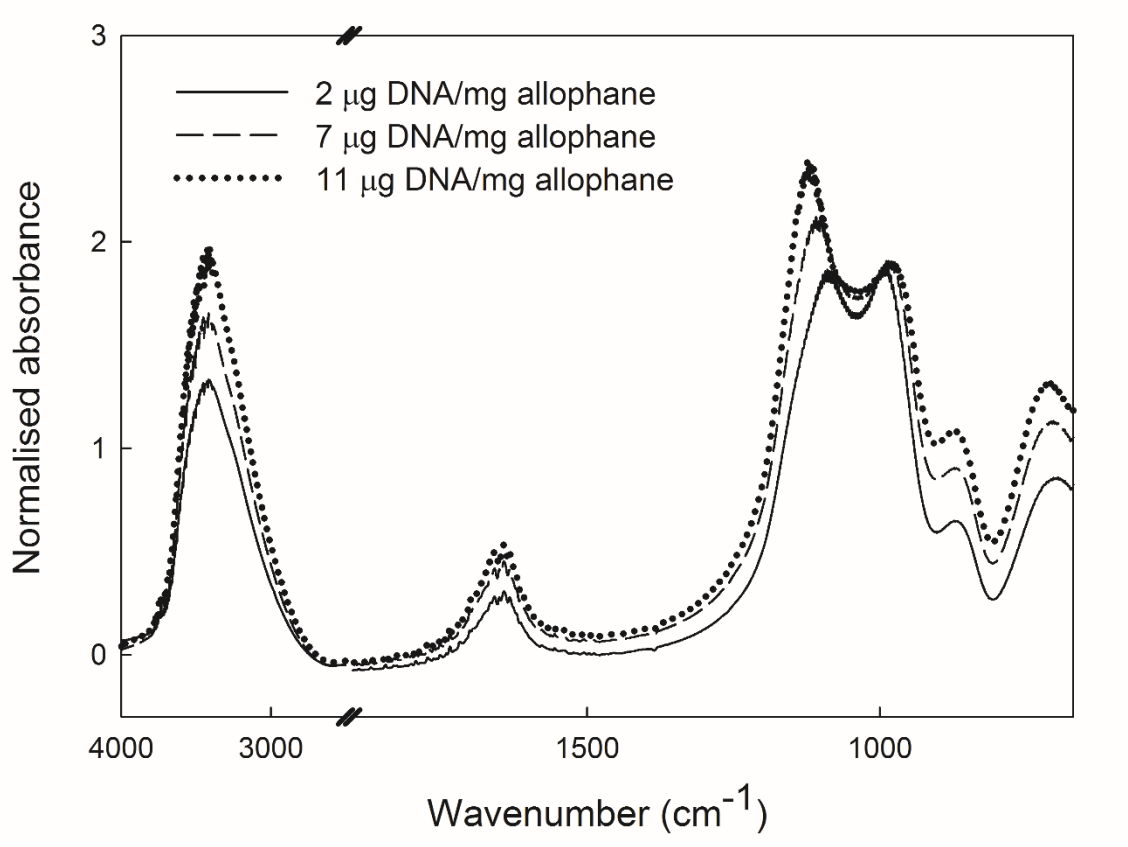

Fig. 8. Normalized infrared spectra for three allophane-DNA complexes with 2 (0.2%), 7 (0.7%), and 11 (1.1%) μg mg^{-1} of DNA additions.

3.5. Formation of allophane nano- and microaggregates and physical adsorption of DNA within pores

During DNA adsorption on synthetic allophane, it was observed that chemical adsorption of DNA on allophane brought about further aggregation/complexation of allophane nanoaggregates simultaneously (Fig. 9) so that the size of allophane nanoaggregates increased to micron-sized aggregates (microaggregates). This phenomenon has been attributed to the chemical adsorption of allophane nanoaggregates on DNA strands, as described by Matsuura et al. (2013), followed by conjoining of these aggregates by the polymeric DNA, with porous allophane microaggregates formed as a result. The microaggregates comprised assemblages of allophane nanoaggregates with numerous spaces (pores) of both nano- and submicron scale. Consequently, DNA fragments could be readily enclosed during the formation of allophane microaggregates, or adsorbed within the nanopores between allophane spherules (i.e., within inter-spherule spaces) or within nano- or submicropores between allophane nanoaggregates (i.e., within inter-nanoaggregate spaces), effectively as a form of physical adsorption as noted earlier.

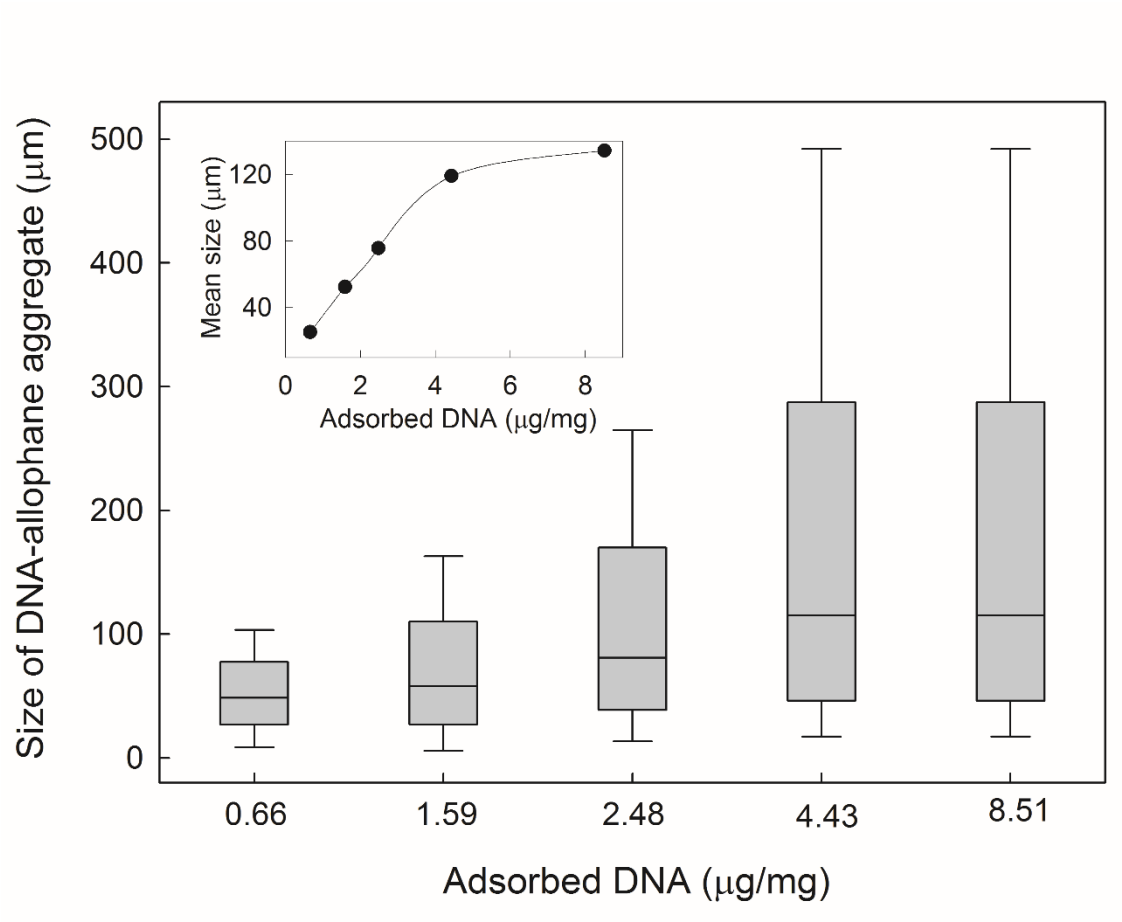

516

517 **Fig. 9.** Size distribution of allophane-DNA aggregates responding to gradually increasing additions
518 of DNA. The 50-allophane was used for this set of experiments. The allophane-DNA aggregates
519 (with differing amounts of DNA additives) were vigorously homogenized in a stirring unit, and
520 hence are demonstrably stable, being unable to be broken down easily. The concentration of DNA
521 added and the mean sizes of the allophane-DNA aggregates are reported alongside each histogram.

522

523 The size of allophane-DNA clusters increased with the addition of DNA (Fig. 9). Allophane
524 microaggregates could be up to 500 μm in diameter and the dominant size of such aggregates with
525 high DNA loading (>4.4 μg DNA per mg allophane) onto synthetic allophane was 100−300 μm.
526 Increasing the DNA adsorbed from 4.4 μg mg^{-1} to 8.5 μg mg^{-1} had no significant impact on the
527 overall size distribution of aggregates, but the result showed a reduction in the volume of

528 nanoaggregates <100 μm in diameter and a predominance of microaggregates with a size range
529 100−300 μm in diameter.

530 The DNA adsorption isotherm on synthetic allophane (Fig. 3) reflected the fact that further
531 adsorption became weak when adsorbed DNA was more than 6 μg mg^{-1} allophane (0.6%), which
532 could be attributable to the saturation of the DNA chemisorption on the surface of allophane
533 spherules and then physical adsorption of DNA in nano- or submicropores within and between
534 allophane nanoaggregates. The DNA uptake by synthetic allophane eventually attained up to 34 μg
535 mg^{-1} allophane (3.4%) whilst the allophane aggregates had continuously grown up to 500 μm in
536 diameter and inter-nanoaggregate spaces had become saturated with DNA. Hence the proportion of
537 chemically-adsorbed DNA to physically-adsorbed DNA is 6 to 28 (34 minus 6), indicating that
538 ~80% of DNA is adsorbed physically in nano- and submicropores.

539 Oades and Waters (1991) showed that soil microaggregates are bound together into
540 macroaggregates by organic matter in most soils, and later Six et al. (2000b) further demonstrated
541 that macroaggregates sequester 1.65 times more carbon than microaggregates. Using an
542 experimental approach earlier, Churchman and Tate (1987) showed that the stability of
543 macroaggregates in allophanic soils on tephra is highly related to carbon content in such soils.
544 Aggregates at nano- and micron scales have also been found to be crucial in helping to govern
545 carbon sequestration in Andisols (Huygens et al., 2005; Asano and Wagai, 2014) in which the large
546 allophane aggregates possess higher volumes of inter-nanoaggregate interstice and hence more
547 room for the physical storage of carbon than in small aggregates. In Fig. 9 it is shown that allophane
548 nanoaggregates could be assembled by DNA molecules acting as strong binding agents, and such
549 aggregation has enabled much DNA to be adsorbed by the allophane microaggregates in the spaces
550 (nano- and submicropores) between aggregates rather than just on the limited aluminol groups on
551 allophane spherules – i.e., physical adsorption within and between allophane aggregates seems to

552 account for much more DNA sequestration than chemical adsorption directly on the surfaces of
553 allophane spherules.

554 It is therefore proposed that environmental DNA in Andisols or allophane-rich soils could be
555 adsorbed by (1) allophane directly via chemisorption, (2) humic acid (or organic matter) covering
556 on allophane and then attached to allophane indirectly, and (3) pores within and between allophane
557 nanoaggregates (inter-spherule and inter-nanoaggregate spaces) via physical adsorption (Fig. 10), of
558 which physical adsorption is considered to be the crucial mechanism allowing substantial
559 environmental DNA to be sequestered in such soil materials because of the high porosity of
560 allophane aggregates. The stability of the allophane-DNA complexes was noticeable because the
561 allophane-DNA microaggregates could not be broken up by turbulent stirring, indicating that DNA
562 (and hence organic matter as well in the natural soil system) would likely be well protected and
563 stored within allophane aggregates. Natural humus-allophane aggregates in Andisols are similarly
564 very stable (e.g. Goh, 1980, 2004; Nanzyo, 2002; Ugolini and Dahlgren, 2002; Matus et al., 2014).
565 The pores at nano- or submicrometre scale between allophane spherules or within aggregates seem
566 to be the main reservoir for DNA adsorption and probably a refuge for DNA because some of the
567 pores are so small (~2−100 nm) that they are not accessible to enzymes or microbes.

568

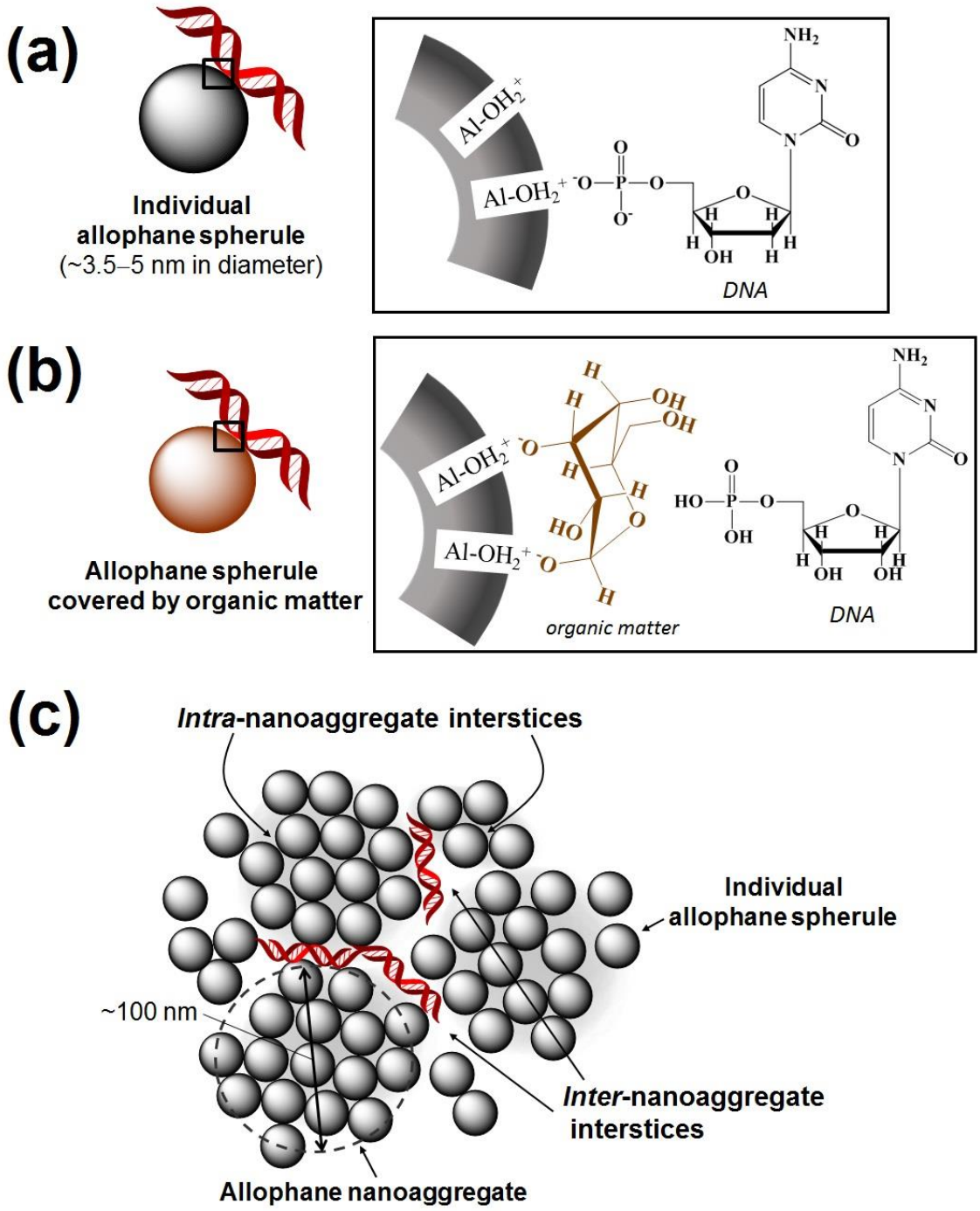

Fig. 10. Illustration of proposed mechanisms for chemical and physical adsorption of DNA by nanocrystalline allophane spherules and allophane nanoaggregates: (A) direct chemical adsorption of DNA on allophane through the phosphate group of DNA; (B) indirect chemical adsorption of DNA on a covering of organic matter on allophane; and (C) physical adsorption of DNA in the spaces (nano- to submicropores) of allophane nanoaggregates and microaggregates (modified after Huang et al., 2014, p. 165, with kind permission of Springer). The natural DNA fragment is ~20 Å (2 nm) in diameter and the DNA grooves (spaces between helical strands) are 12−22 Å (1.2−2.2 nm) wide.

578 Therefore, the formation of allophane aggregates and the physical adsorption of DNA within
579 nanopores amidst allophane aggregates may be indicative of better preservation of environmental
580 DNA in natural allophanic soil materials than in other (non-allophanic) mineral soils (Rawlence et
581 al., 2014).

582

583 *3.6. Implications for carbon sequestration in Andisols*

584 The findings relating to DNA may also pertain to soil organic matter and organic carbon in
585 that the porous and stable allophane aggregates potentially allow much organic carbon to be
586 adsorbed physically, being encapsulated within the small spaces (pores), thereby leading to slow
587 carbon turnover in Andisols (Parfitt et al., 2002; Parfitt, 2009; Baisden et al., 2010, 2013).
588 Previously, the high organic carbon content of Andisols had been ascribed mainly to the very high
589 SSA and the variable surface charge characteristics associated with allophane (e.g. Harsh, 2012;
590 McDaniel et al., 2012), and to the strong propensity of allophane to form nanoaggregates up to 100
591 nm in diameter that enable carbon to become stabilized and protected (e.g. Goh, 2004; Chevallier et
592 al., 2010; Calabi-Floody et al., 2011; Matus et al., 2014). In some Andisols, carbon, mainly as
593 humus, becomes stabilized through complexation and precipitation with Al (e.g. Percival et al.,
594 2000; Yuan et al., 2000; Nanzyo, 2002; Basile-Doelsch et al., 2005; Chevaliier et al., 2010;
595 McDaniel et al., 2012; Takahashi and Dahlgren, 2016). However, the findings obtained here with
596 respect to DNA – up to 80% of which was physically adsorbed (and presumably protected) on
597 synthetic allophane – provide a mechanism to explain carbon sequestration more specifically in
598 Andisols: a high proportion of organic carbon is encapsulated within myriads of small to tiny pores,
599 effectively within a nanolabyrinth, both (1) amidst nanoaggregates of allophane spherules (inter-
600 spherule spaces), and (2) in pores between nanoaggregates (inter-nanoaggregate spaces) within
601 microaggregates, of which the microaggregates possess higher volumes of interstitial space for

carbon adsorption than nanoaggregates. For the synthetic allophane examined in this study, the dominant pore size of the inter-spherule spaces was ~3 nm (nanopores), and that of the inter-nanoaggregate spaces (nano- to submicropores) was ~30 to 100 nm. For natural allophane, the equivalent pore dimensions within and between nanoaggregates were ~2 nm and ~50−500 nm (based on micrographs of natural allophane), respectively. Such sizes ranges amidst very stable aggregates (both nano- and microaggregates) provide natural 'havens' for organic carbon to be encapsulated more or less permanently, free from attack because the Al-rich allophane spherules encircling the nanopores are non-bioavailable to most microorganisms (because of Al toxicity), enzymes themselves may be adsorbed, microbes are deprived of phosphorus (because of strong P retention) (Tate and Theng, 1980; Ugolini and Dahlgren, 2002; Matus et al., 2014), and because the nanopores and their openings are both too small and too tortuous for enzymes and microbes to access.

Using small angle X-ray scattering (SAXS), Chevallier et al. (2010) showed for Andisols in Martinique (French West Indies) that an increasingly tortuous nanopore network (defined as the extent of fractal range or cluster, ξ/a, where ξ is the size of allophane aggregates and a is 3.5 nm, the mean size of natural allophane spherules) resulted in decreasing carbon bioavailability. A larger ξ/a ratio indicates a more tortuous pore network. Similar research was undertaken by Woignier et al. (2008). Filimonova et al. (2011) used ^{129}Xe nuclear magnetic resonance (NMR) spectroscopic studies of xenon gas adsorption of a non-allophanic Andisol (i.e. an Andisol dominated by Al- and Fe-humus complexes: Takahashi and Dahlgren, 2016) to show that its porous structure comprised interconnected micro- and mesopores formed by agglomerated nano-sized Al-rich clusters, the micropores, critically, being very narrow (~0.44–0.88 nm). In the current study, the synthetic allophane spherules were ~10−15 nm in diameter (mean size ~12.5 nm), and the allophane nanoaggregates were between ~50 and ~100 nm in diameter, and so it is estimated that the ξ/a ratio is between 4 (50/12.5) and 8 (100/12.5). Chevallier et al. (2010) reported that a ξ/a ratio of about

627 10 “implies the existence of a large tortuous labyrinth built of allophane particles” (p. 184). Thus,
628 assuming the results for natural allophane apply to the synthetic allophane in the current study, then
629 the ξ/a ratios of ~4 to 8 imply that pore networks in the synthetic allophane nanoaggregates
630 (without any added DNA) have at least a moderately high degree of tortuosity.

631 Parallel conclusions have been reported previously in various studies that examined the
632 nature of the relationship between minerals and organic carbon/organic matter in non-allophanic
633 soils (e.g. Six et al., 2000a, 2000b; Lehmann et al., 2007; Baldock and Broos, 2012; Churchman
634 and Lowe, 2012). For example, Mayer and Xing (2001), Kaiser and Guggenberger (2003), and
635 Chenu and Plante (2006) concluded that most organic matter was stabilized in soils by close
636 associations with clays in very small microaggregates, either through adsorption or by entrapment
637 (occlusion). Wan et al. (2007), using scanning transmission X-ray microscopy (STXM), showed
638 that organic matter existed as distinct particles within microaggregates more typically than as
639 coatings on minerals. And McCarthy et al. (2008), who used SAXS to directly observe pores and
640 their constituents, found that most organic matter was held within pores, and that it was
641 encapsulated, rather than adsorbed, by minerals. Consequently, the results of the current study
642 relating to DNA adsorption on synthetic allophane strongly imply that such mechanisms of
643 encapsulation of organic carbon within pores in nanoaggregates apply to allophanic soils including
644 Andisols.

645 In comparing the world’s soil orders based on *Soil Taxonomy* (with the exclusion of
646 Histosols) (Soil Survey Staff, 1999), the foremost ability of Andisols to sequester carbon, and the
647 primacy of allophane nanominerals rather than long-range-order and other crystalline clay minerals
648 in affecting such sequestration, are therefore attributable largely to the very high fractal-scale
649 porosity (at nano- and submicron scales) and stability of their constituent nanoaggregates and
650 microaggregates.

4. Conclusions

(1) The synthetic allophane spherules made in this study were uniformly 10−15 nm in diameter and with a SSA up to 374 $m^2 g^{-1}$. Generally, 1 mg of synthetic allophane could adsorb up to 34 μg of salmon-sperm DNA in total.

(2) P XANES and IR spectra for salmon-sperm DNA-allophane complexes affirmed that the chemical adsorption of DNA by allophane is through its phosphate groups (direct chemical adsorption of DNA on allophane spherules). The DNA adsorption on allophane induced an alteration of the surface chemistry of allophane whereby the characteristic Si−O−Al stretching frequency of allophane shifted from 1020 cm^{-1} to 990 cm^{-1}. This alteration and shift could be attributable to either the change of interatomic distances of the allophane wall or the precipitation of aluminium phosphates on the surface of allophane, or both.

(3) Humic acid hampered the DNA adsorption capacity on synthetic allophane by occupying the active sites on allophane and suppressing the charge relocation between DNA and humic acid-rich allophane. However, some ligands of humic acid bound to DNA chemically through its phosphate groups and DNA became attached to allophane spherules indirectly (indirect chemical adsorption on allophane).

(4) The adsorptive sites on the surface of allophane spherules became saturated despite the addition of only small amounts of DNA (~2−6 μg mg^{-1} allophane), but much more DNA (up to 28 μg mg^{-1}, ~80% of the total DNA adsorbed) was able to be adsorbed by allophane physically (i.e., in nanopores and submicropores) when the porous allophane-DNA aggregates (including nano- and microaggregates) were formed. The aggregation of DNA and allophane spherules and great stability of such aggregates thus explain why allophanic soil materials are able to sequester much DNA, and hence slow the degradation of DNA in such materials.

(5) These findings relating to DNA very likely appertain to soil organic matter in that the stable, highly porous allophane nano- and microaggregates allow much organic matter and organic carbon (potentially up to ~80%) to be adsorbed physically. The carbon is effectively encapsulated and protected within a nanolabyrinthic network of nanopores (<100 nm) and submicropores (100−500 nm), enhanced because of the network's high degree of tortuosity, thereby leading to the especially slow turnover of carbon in Andisols and other allophanic soils.

Abbreviations

BET, Brunauer-Emmett-Teller; BJH, Barrett-Joyner-Halenda; C, carbon; DI, deionised; DNA, deoxyribonucleic acid; FTIR, Fourier transform infrared; HA, humic acid; IR, infrared; NMR, nuclear magnetic resonance; NSRRC, National Synchrotron Radiation Research Center; RNA, ribonucleic acid; SAXS, small angle X-ray scattering; SSA, specific surface area; STXM, scanning transmission X-ray microscopy; WL, white line; XANES, X-ray absorption near-edge structure.

Acknowledgements

This research was supported largely by the New Zealand Marsden Fund, administered through the Royal Society of New Zealand, for a project entitled "New views from old soils: testing the reconstruction of environmental and climatic change using genetic signals preserved in buried paleosols" (contract UOW1006 to D.J. Lowe), and in part by a University of Waikato doctoral scholarship to Y-T. Huang. Prof Shin-Ichiro Wada (Kyushu University) is thanked for advice on allophane synthesis, and Dr Yao-Chang Lee and Dr Ling-Yun Jang at the National Synchrotron Radiation Research Center (NSRRC), Taiwan, are thanked for their instructions and support relating to infrared spectroscopy and P XANES spectroscopy, respectively. Helen Turner of the Microscope Unit, University of Waikato, and staff at the National Sun Yat-Sen University, Taiwan,

helped acquire the TEM images. Prof Hsing-Cheng Hsi is thanked for his help with BET analysis. Support staff at the School of Science, University of Waikato, and at NSRRC, are acknowledged for providing excellent working conditions and assistance. Various publishers are especially thanked for granting permissions to reproduce figures as noted in the text. Two anonymous reviewers and the editor (F. Bergaya) are thanked for their useful comments.

References

Abidin, Z., Matsue, N., Henmi, T., 2007. Differential formation of allophane and imogolite: experimental and molecular orbital study. Journal of Computer-aided Materials Design 14, 5-18.

Allbrook, R.F., 1983. Some physical properties of allophane soils from the North Island, New Zealand. New Zealand Journal of Science 26, 481-492.

Allbrook, R.F., 1985. The effect of allophane on soil properties. Applied Clay Science 1, 65-69.

Allbrook, R.F., 1992. Shrinkage of some New Zealand soils and its implications for soil physics. Australian Journal of Soil Research 31, 111-118.

Asano, M., Wagai, R., 2014. Evidence of aggregate hierarchy at micro- to submicro scales in an allophanic Andisol. Geoderma 216, 62-74.

Baisden, W.T., Parfitt, R.L., Ross, C.W., 2010. Radiocarbon evidence for contrasting soil carbon dynamics in an Andisol and non-Andisol pasture soil comparison. Journal of Integrated Field Science 7, 59-64.

Baisden, W.T., Parfitt, R.L., Ross, C., Schipper, L.A., Canessa, S., 2013. Evaluating 50 years of time-series soil radiocarbon data: towards routine calculation of robust C residence times. Biogeochemistry 112, 129-137.

Baldock, J.A., Broos, K., 2012. Soil organic matter, in: Huang, P.M., Li, Y., Sumner, M.E. (Eds.), Handbook of Soil Sciences, second edition, Vol. 1: Properties and Processes. CRC Press, Boca Raton, FL, pp. 11.1-11.52.

Barrett, E.P., Joyner, L.G.,Halenda, P.P., 1951. The determination of pore volume and area distributions in porous substances. I. Computations from nitrogen isotherms. Journal of The American Chemical Society 73, 373-380.

727 Basile-Doelsch, Amundson, R., Stone, W.E.E., Masiello, C.A., Bottero, J.Y., Colin, F., Borschneck,
728 D., Meunier, J.D., 2005. Mineralogical control of organic carbon dynamics in a volcanic ash
729 soil on La Réunion. European Journal of Soil Science 56, 689-703.
730 Bergaya, F., Lagaly, G., 2013. General introduction: clays, clay minerals, and clay science, in:
731 Bergaya, F., Lagaly, G. (Eds.), Handbook of Clay Science, second edition, Part A:
732 Fundamentals. Elsevier, Amsterdam, Developments in Clay Science 5A, pp. 1-19.
733 Blakemore, L.C., Searle, P.L.,Daly, B.K., 1987. Methods for chemical analysis of soils. New
734 Zealand Soil Bureau Scientific Report 80, 103 pp.
735 Blanco-Canqui, H., Lal, R., 2004. Mechanisms of carbon sequestration in soil aggregates. Critical
736 Reviews in Plant Sciences 23, 481-504.
737 Brown, W., Poon T., 2005. Infrared spectroscopy, in: Brown, W., Poon, T. (Eds.), Introduction to
738 Organic Chemistry, third edition. Wiley, New Jersey, pp. 304-328.
739 Brunauer, S., Emmett, P.H., Teller, E., 1938. Adsorption of gases in multimolecular layers. Journal
740 of the American Chemical Society 60, 309-319.
741 Buurman, P., Peterse, F., Almendros Martin, G., 2007. Soil organic matter chemistry in allophanic
742 soils: a pyrolysis-GC/MS study of a Costa Rican Andosol catena. European Journal of Soil
743 Science 58, 1330-1347.
744 Cai, P., Huang, Q., Jiang, D., Rong, X., Liang, W., 2006. Microcalorimetric studies on the
745 adsorption of DNA by soil colloidal particles. Colloids and Surfaces B: Biointerfaces 49, 49-
746 54.
747 Cai, P., Huang, Q., Zhu, J., Jiang, D., Zhou, X., Rong, X., Liang, W., 2007. Effects of low-
748 molecular-weight organic ligands and phosphate on DNA adsorption by soil colloids and
749 minerals. Colloids and Surfaces B: Biointerfaces 54, 53-59.
750 Calabi-Floody, M., Bendall, J.S., Jara, A.A., Welland, M.E., Theng, B.K.G., Rumpel, C., de la Luz
751 Mora, M., 2011. Nanoclays from an Andisol: extraction, properties and carbon stabilization.
752 Geoderma 161, 159-167.
753 Calabi-Floody, M., Rumpel, C., de la Luz Mora, M. ., 2014. Stability of soil organic matter in
754 particle size fractions in top and subsoil of Chilean Andisols. Congress symposium C1.3:
755 Volcanic soils: distinctive properties and management. Proceedings of the 20th World Congess
756 of Soil Science (www.20wcss.org), Abstract Online Access System, Jeju, South Korea.
757 Chenu, C., Plante, A.F., 2006. Clay-sized organo-mineral complexes in a cultivation
758 chronosequence: revisiting the concept of the ‘primary organo-mineral complex.’ European
759 Journal of Soil Science 57, 596-607.

760 Chevallier, T., Woignier, T., Toucet, J., Blanchart, E., 2010. Organic carbon stabilization in the
761 fractal pore structure of Andosols. Geoderma 159, 182-188.
762 Churchman, G.J., Tate, K.R., 1987. Stability of aggregates of different size grades in allophanic
763 soils from volcanic ash in New Zealand. Journal of Soil Science 38, 19-27.
764 Churchman, G.J., Lowe, D.J., 2012. Alteration, formation, and occurrence of minerals in soils, in:
765 Huang, P.M., Li, Y., Sumner, M.E. (Eds.), Handbook of Soil Sciences, second edition, Vol. 1:
766 Properties and Processes. CRC Press, Boca Raton, FL, pp. 20.1-20.72.
767 Creton, B., Bougeard, D., Smirnov, K.S., Guilment, J., Poncelet, O., 2008. Structure model and
768 computer modeling study of allophane. Journal of Physical Chemistry C 112, 358-364.
769 Dahlgren, R.A., Saigusa, M., Ugolini, F.C., 2004. The nature, properties and management of
770 volcanic soils. Advances in Agronomy 82, 113-182.
771 Delmelle, P., Opfergelt, S., Cornelis, J.-T., Ping, C.-L., 2015. Volcanic soils, in: Sigurdsson, H.,
772 Houghton, B.F., Rymer, H., Stix, J., McNutt, S. (Eds.), Encyclopedia of Volcanoes, second
773 edition. Academic Press, San Diego, pp. 1253-1264.
774 Elliot, E.T., 1986. Aggregate structure and carbon, nitrogen, and phosphorus in native and
775 cultivated soils. Soil Science Society of America Journal 50, 627-633.
776 Farmer, V.C., 1968. Infrared spectroscopy in clay mineral studies. Clay Minerals 7, 373-387.
777 Filimonova, S., Nossov, A., Dümig, A., Gédéon, A., Kögel-Knabner, I., Heike Knicker, H., 2011.
778 Evaluating pore structures of soil components with a combination of “conventional” and
779 hyperpolarised ^{129}Xe NMR studies. Geoderma 162, 96-106.
780 Goh, K.M., 1980. Dynamics and stability of organic matter, in: Theng, B.K.G. (Ed.), Soils with
781 Variable Charge. New Zealand Society of Soil Science, Lower Hutt, pp. 373-393.
782 Goh, K.M., 2004. Carbon sequestration and stabilization in soils: implications for soil productivity
783 and climate change. Soil Science and Plant Nutrition 50, 467-476.
784 Gray, C.W., Allbrook, R.F., 2002. Relationships between shrinkage indices and soil properties in
785 some New Zealand soils. Geoderma 108, 287-299.
786 Harsh, J., 2012. Poorly crystalline aluminosilicate clay minerals, in: Huang, P.M., Li, Y., Sumner,
787 M.E. (Eds.), Handbook of Soil Sciences, second edition, Vol. 1: Properties and Processes.
788 CRC Press, Boca Raton, FL, pp. 23.1-23.13.
789 Hashizume, H., Theng, B.K.G., 2007. Adenine, adenosine, ribose and 5′-amp adsorption to
790 allophane. Clays and Clay minerals 55, 599-605.
791 Henmi, T., Wada, K., 1976. Morphology and composition of allophane. American Mineralogist 61,
792 379-390.

793 Hesterberg, D., 2010. Macroscale chemical properties and X-ray absorption spectroscopy of soil
794 phosphorus, in: Singh, B., Grafe, M. (Eds.), Synchrotron-based Techniques in Soils and
795 Sediments. Elsevier, Amsterdam, pp. 313-356.
796 Huang, Y.-T., Churchman, J.G., Lowe, D.J., Rawlence, N.J., Schipper, L., Cooper, A., 2012.
797 Evaluating the charater and preservation of DNA within allophane clusters in buried soils on
798 Holocene tephras, northern New Zealand, in: Churchman, G.J., Cresswell, R., Singh, B. (Eds.),
799 Proceedings of Combined Australian Regolith Geoscientists Association and Australian Clay
800 Minerals Society Conference., Mildura, Australia, pp. 121-124.
801 Huang, Y.-T., Lowe, D.J., Churchman, G.J., Schipper, L., Rawlence, N.J., Cooper, A., 2014.
802 Carbon storage and DNA adsorption in allophanic soils and paleosols, in: Hartemink, A.E.,
803 McSweeney, K. (Eds.), Soil Carbon. Springer, New York, pp. 163-172.
804 Huygens, D., Boeckx, P., Van Cleemput, O., Oyarzún, C., Godoy, R., 2005. Aggregate and soil
805 organic carbon dynamics in south Chilean Andisols. Biogeosciences, European Geosciences
806 Union 2, 159-174.
807 Iyoda, F., Hayashi, S., Arakawa, S., John, B., Okamoto, M., Hayashi, H., Yuan, G., 2012. Synthesis
808 and adsorption characteristics of hollow spherical allophane nano-particles. Applied Clay
809 Science 56, 77-83.
810 Karube, J., Nakaishi, K. Sugimoto, H., Fujihira, M., 1996. Size and shape of allophane particles in
811 dispersed aqueous systems. Clays and Clay Minerals 44, 485-491.
812 Kaufhold, S., Dohrmann, R., Abidin, Z., Henmi, T., Matsue, N., Eichinger, L., Kaufhold, A., Jahn,
813 R., 2010. Allophane compared with other sorbent minerals for the removal of fluoride from
814 water with particular focus on a mineable Ecuadorian allophane. Applied Clay Science 50, 25-
815 33.
816 Khare, N., Hesterberg, D., Martine, J.D., 2005. XANES investigation of phosphate sorption in
817 single and binary systems of iron and aluminum oxide minerals. Environmental Science and
818 Technology 39, 2152-2160.
819 Kaiser, K., Guggenberger, G., 2003. Mineral surfaces and organic matter. European Journal of Soil
820 Science 54, 219-236.
821 Lehmann, J., Kinyangi, J., Solomon, D., 2007. Organic matter stabilization in soil microaggregates:
822 implications from spatial heterogeneity of organic carbon contents and carbon forms.
823 Biogeochemistry 85, 45-57.
824 Lehmann, J., Solomon, D., 2010. Organic carbon chemistry in soils observed by synchrotron-based
825 spectroscopy, in: Singh, B., Grafe, M. (Eds.), Synchrotron-based Techniques in Soils and
826 Sediments. Elsevier, Amsterdam, pp. 289-312.

827 Maeda, T., Takenaka, H., Warkentin, B.P., 1977. Physical properties of allophane soils. Advances
828 in Agronomy 29, 229-264.
829 Matsuura, Y., Iyoda, F., Arakawa, S., John, B., Okamoto, M.,Hayashi, H., 2013. DNA adsorption
830 characteristics of hollow spherule allophane nano-particles. Materials Science and Engineering:
831 C 33, 5079-5083.
832 Matsuura, Y., Arakawa, S., Okamoto, M., 2014. Single-stranded DNA adsorption characteristics by
833 hollow spherule allophane nano-particles: pH dependence and computer simulation. Applied
834 Clay Science 101, 591-597.
835 Matus, F., Rumpel, C., Neculman, R., Panichini, M., Mora, M.L., 2014. Soil carbon storage and
836 stabilisation in andic soils: a review. Catena 120, 102-110.
837 Mayer, L.M., Xing, B., 2001. Organic matter-surface area relationships in acid soils. Soil Science
838 Society of America Journal 65, 250-258.
839 McCarthy, J.F., Ilavsky, J., Jastrow, J.F., Mayer, L.M., Perfect, E., Zhuang, J., 2008. Protection of
840 organic matter in soil microaggregates via restructuring of aggregate porosity and filling of
841 pores with accumulating organic matter. Geochimica et Cosmochimica Acta 72, 4725-4744.
842 McDaniel, P.A., Lowe, D.J., Arnalds, O., Ping, C.-L., 2012. Andisols, in: Huang, P.M., Li, Y.,
843 Sumner, M.E. (Eds.), Handbook of Soil Sciences, second edition, Vol. 1: Properties and
844 Processes. CRC Press, Boca Raton, FL, pp. 33.29-33.48.
845 Nanzyo, M., 1984. Diffuse reflectance infrared spectra of phosphate sorbed on alumina gel. Journal
846 of Soil Science 35, 63-69.
847 Nanzyo, M., 2002. Unique properties of volcanic ash soils. Global Environmental Research 6, 99-
848 112.
849 Neimark, A.V., Ravikovitch, P.I., Vishnyakov, A., 2000. Adsorption hysteresis in nanopores.
850 Physical Review E 62, R1493-R1496.
851 Oades, J.M., Waters, A.G., 1991. Aggregate hierarchy in soils. Australian Journal of Soil Research
852 29, 815-828.
853 Ogram, A., Sayler, G.S., Gustin, D., Lewis, R.J., 1988. DNA adsorption to soils and sediments.
854 Environmental Science and Technology 22, 982-984.
855 Ohashi, F., Wada, S.I., Suzuki, M., Maeda, M., Tomura, S., 2002. Synthetic allophane from high-
856 concentration solutions: nanoengineering of the porous solid. Clay Minerals 37, 451-456.
857 Paget, E., Monrozier, L.J., Simonet, P., 1992. Adsorption of DNA on clay minerals: protection
858 against DNaseI and influence on gene transfer. FemS Microbiology Letters 97, 31-39.
859 Parfitt, R.L., 1989. Phosphate reactions with natural allophane, ferrihydrite and goethite. Journal of
860 Soil Science 40, 359-369.

Parfitt, R.L., 1990. Allophane in New Zealand – a review. Australian Journal of Soil Research 28, 343-360.

Parfitt, R.L., 2009. Allophane and imogolite: role in soil biogeochemical processes. Clay Minerals 44, 135-155.

Parfitt, R.L., Henmi, T., 1980. Structure of some allophanes from New Zealand. Clays and Clay Minerals 28, 285-294.

Parfitt, R.L., Henmi, T., 1982. Comparison of an oxalate-extraction method and an infrared spectroscopic method for determining allophane in soil clays. Soil Science and Plant Nutrition 28, 183-190.

Parfitt, R.L., Wilson, A.D., 1985. Estimation of allophane and halloysite in three sequences of volcanic soils, New Zealand. Catena Supplement 7, 1-8.

Parfitt, R.L., Yuan, G., 2012. Does clay stabilise organic matter in New Zealand soils? Soil Horizons 21, 11.

Parfitt, R.L., Furkert, R.J., Henmi, T., 1980. Identification and structure of two types of allophane from volcanic ash soils and tephra. Clays and Clay Minerals 28, 328-334.

Parfitt, R.L., Parshotam, A., Salt, G.J., 2002. Carbon turnover in two soils with contrasting mineralogy under long-term maize and pasture. Australian Journal of Soil Research 40, 127-136.

Percival, H.J., Parfitt, R.L., Scott, N.A., 2000. Factors controlling soil carbon levels in New Zealand grasslands: is clay content important? Soil Science Society of America Journal 64, 1623-1630.

Ravel, B., Newville, M., 2005. ATHENA, ARTEMIS, HEPHAESTUS: data analysis for X-ray absorption spectroscopy using IFEFFIT. Journal of Synchrotron Radiation 12, 537-541.

Rawlence, N.J., Lowe, D.J., Wood, J.R., Young, J.M., Churchman, G.J., Huang, Y.-T., Cooper, A., 2014. Using palaeoenvironmental DNA to reconstruct past environments: progress and prospects. Journal of Quaternary Science 29, 610-626.

Rousseaux, J.M., Warkentin, B.P., 1976. Surface properties and forces holding water in allophane soils. Soil Science Society of America Journal 40, 446-451.

Saeki, K., Sakai, M., 2009. The influence of soil organic matter on DNA adsorptions on Andosols. Microbes and Environments 24, 175-179.

Saeki, K., Kunito, T., Sakai, M., 2010a. Effects of pH, ionic strength, and solutes on DNA adsorption by andosols. Biology and Fertility of Soils 46, 531-535.

Saeki, K., Sakai, M., Wada, S.-I., 2010b. DNA adsorption on synthetic and natural allophanes. Applied Clay Science 50, 493-497.

894 Saeki, K., Ihyo, Y., Sakai, M., Kunito, T., 2011. Strong adsorption of DNA molecules on humic
895 acids. Environmental Chemistry Letters 9, 505-509.
896 Shin, E.W., Han, J.S., Jang, M., Min, S.-H., Park, J.K., Rowell, R.M., 2004. Phosphate adsorption
897 on aluminum-impregnated mesoporous silicates: surface structure and behavior of adsorbents.
898 Environmental Science and Technology 38, 912-917.
899 Six, J., Elliott, E.T., Paustian, K., 2000a. Soil macroaggregate turnover and microaggregate
900 formation: a mechanism for C sequestration under no-tillage agriculture. Soil Biology and
901 Biochemistry 32, 2099-2103.
902 Six, J., Paustian, K., Elliott, E.T., Combrink, C., 2000b. Soil structure and organic matter: I.
903 Distribution of aggregate-size classes and aggregate-associated carbon. Soil Science Society of
904 America Journal 64, 681-689.
905 Sochan, A., Bieganowski, A., Ryżak, M., Dobrowolski, R., Bartmiński, P., 2012. Comparison of
906 soil texture determined by two dispersion units of Mastersizer 2000. International Agrophysics
907 26, 99-102.
908 Soil Survey Staff, 1999. Soil Taxonomy − a basic system of soil classification for making and
909 interpreting soil surveys, second edition. USDA-NRCS Agricultural Handbook 436. U.S.
910 Government Printing Office, Washington, DC, 869 pp.
911 Sposito, G., 1989. Soil adsorption phenomena, in: Sposito, G. (Ed.), The Chemistry of Soils.
912 Oxford University Press, Oxford, pp. 148-169.
913 Tahoun, S.A., 2014. Infrared spectroscopy in research of clay mineralogy and soil chemistry: A
914 tribute to pioneers and an extended frontier in the context of biomolecules synthesis. Applied
915 Clay Science 93-94, 35-37.
916 Takahashi, T., Dahlgren, R.A., 2016. Nature, properties and function of aluminium–humus
917 complexes in volcanic soils. Geoderma 263, 110-121.
918 Tate, K.R., Theng, B.K.G., 1980. Organic matter and its interactions with inorganic soil
919 constituents, in: Theng, B.K.G. (Ed), Soils with Variable Charge. New Zealand Society of Soil
920 Science, Lower Hutt, pp. 225-249.
921 Terzano, R., Denecke, M.A., Medici, L., 2010. Synchrotron radiation in soil and geosciences.
922 Journal of Synchrotron Radiation 17, 147-148.
923 Torn, M.S., Trumbore, S.E., Chadwick, O.A., Vitousek, P.M., Hendricks, D.M., 1997. Mineral
924 control of soil organic carbon storage and turnover. Nature 389, 170-173.
925 Ugolini, F.C., Dahlgren, R.A., 2002. Soil development in volcanic ash. Global Environmental
926 Research 6, 69-81.

927 Wada, K., 1980. Mineralogical characterisics of Andisols, in: Theng, B.K.G. (Ed.), Soils with
928 Variable Charge. New Zealand Society of Soil Science, Lower Hutt, pp. 87-107.
929 Wan, J., Tyliszczak, T., Tokunga, T.K., 2007. Organic carbon distribution, speciation, and
930 elemental correlations within soil microaggregates: applications of STXM and NEXAFS
931 spectroscopy. Geochimica et Cosmochimica Acta 71, 5439-5449.
932 Wells, N., Northey, R.D., 1984. Shearing characteristics of an allophane soil. Clay Science 6, 93-
933 101.
934 Woignier, T., Pochet, G., Doumenc, H., Dieudonné, P., Duffours, L., 2007. Allophane: a natural gel
935 in volcanic soils with interesting environmental properties. Journal of Sol-Gel Science and
936 Technology 41, 25-30.
937 Woignier, T., Morell, M., Primera, J., Duffours, L., 2008. Correlation between large water content
938 and fractal structure in volcanic soils. Proceedings BALWOIS 2008, Water Observation and
939 Information System for Balkan Countries (BALWOIS Project), Ohrid, Republic of Macedonia,
940 27-31 May 2008, pp.1-10.
941 Yuan, G., Wada, S.-I., 2012. Allophane and imogolite nanoparticles in soil and their environmental
942 applications, in: Barnard, A.S., Guo, H. (Eds.), Nature's Nanostructures. Pan Stanford,
943 Singapore, pp. 494-515.
944 Yuan, G., Theng, B.K.G., Parfitt, R.L., Percival, H.J., 2000. Interactions of allophane with humic
945 acid and cations. European Journal of Soil Science 51, 35-41.
946